


D.D. NELSON
J.H. SHORTER
J.B. MCMANUS
M.S. ZAHNISER 

Sub-part-per-billion detection of nitric oxide in air using a thermoelectrically cooled mid-infrared quantum cascade laser spectrometer

Aerodyne Research, Inc., 45 Manning Rd., Billerica, MA 01821-3976, USA

Received: 1 May 2002/Revised version: 6 June 2002
Published online: 21 August 2002 • © Springer-Verlag 2002

ABSTRACT Non-cryogenic, laser-absorption spectroscopy in the mid-infrared has wide applications for practical detection of trace gases in the atmosphere. We report measurements of nitric oxide in air with a detection limit less than 1 nmole/mole (< 1 ppbv) using a thermoelectrically cooled quantum cascade laser operated in pulsed mode at $5.26 \mu\text{m}$ and coupled to a 210-m path length multiple-pass absorption cell at reduced pressure (50 Torr). The sensitivity of the system is enhanced by operating under pulsing conditions which reduce the laser line width to 0.010 cm^{-1} (300 MHz) HWHM, and by normalizing pulse-to-pulse intensity variations with temporal gating on a single HgCdTe detector. The system is demonstrated by detecting nitric oxide in outside air and comparing results to a conventional tunable diode laser spectrometer sampling from a common inlet. A detection precision of $0.12 \text{ ppb Hz}^{-1/2}$ is achieved with a liquid-nitrogen-cooled detector. This detection precision corresponds to an absorbance precision of $1 \times 10^{-5} \text{ Hz}^{-1/2}$ or an absorbance precision per unit path length of $5 \times 10^{-10} \text{ cm}^{-1} \text{ Hz}^{-1/2}$. A precision of $0.3 \text{ ppb Hz}^{-1/2}$ is obtained using a thermoelectrically cooled detector, which allows continuous unattended operation over extended time periods with a totally cryogen-free instrument.

PACS 42.62.Fi; 82.80.Gk; 92.60.Sz

1 Introduction

Tunable infrared laser differential absorption spectroscopy (TILDAS) has been widely used for atmospheric trace-gas detection due to its high sensitivity, good specificity, and fast time response for molecules with resolvable ro-vibrational structure especially in the mid-infrared spectral region containing the stronger fundamental vibrational bands. Wider applicability of the technique has been limited by the cryogenic cooling requirements of lead-salt tunable diode lasers (TDLs), which make them difficult to characterize and less stable with respect to spectral characteristics such as wavelength reproducibility and mode purity. Quantum cascade (QC) or unipolar lasers provide an alternative source

of high-resolution mid-infrared radiation that has overcome some of the difficulties associated with lead-salt diode lasers by providing near-room-temperature operation, single-mode continuous tuning over several wavenumbers, and increased power output. Since QC lasers were first demonstrated [1], they have undergone rapid development [2–4] and been used for a number of applications for atmospheric trace-gas detection in both continuous-wave operation with liquid-nitrogen cooling [5–7] and in pulsed mode with thermoelectric (TE) cooling [8–12]. QC lasers are extremely stable with respect to wavelength drift so that automatic computer control is quite practical. The output power is sufficient to allow the use of thermoelectrically cooled detectors even when coupled into multiple-pass absorption cells with a large number of reflections.

In this paper we demonstrate measurements of nitric oxide in air with a detection limit of less than 1 nmole/mole (< 1 ppbv) using a totally thermoelectrically cooled QC-TILDAS instrument. The method is widely applicable to other trace gases of interest in studies of atmospheric and environmental chemistry, global climate change, as well as industrial process monitoring.

2 Experimental

The experimental system employed for this study combined a commercially available unipolar laser and associated drive electronics, a laser control and signal processing system adapted from our infrared tunable diode laser instruments, and an optical system constructed at Aerodyne for use with tunable diode lasers, including a 210-m path length absorption cell. We have tested the system with both a liquid-nitrogen-cooled detector (Kolmar Technologies, Inc.) and with a thermoelectrically cooled detector (Vigo Systems, Ltd.). A schematic of the experimental system is shown in Fig. 1. The unipolar (quantum cascade) laser as well as the laser pulser and bias circuit were obtained from Alpes Laser (Neuchatel, Switzerland). The laser was of the same design as described by Hofstetter et al. [13]. The laser is grown using the InGaAs material system and includes a distributed-feedback grating. The laser operates between 1880 and 1900 cm^{-1} , in pulsed mode, at a temperature set by a Peltier cooler of between $+10$ and -40° .

 Fax: +1-978/663-4918, E-mail: ddn@aerodyne.com

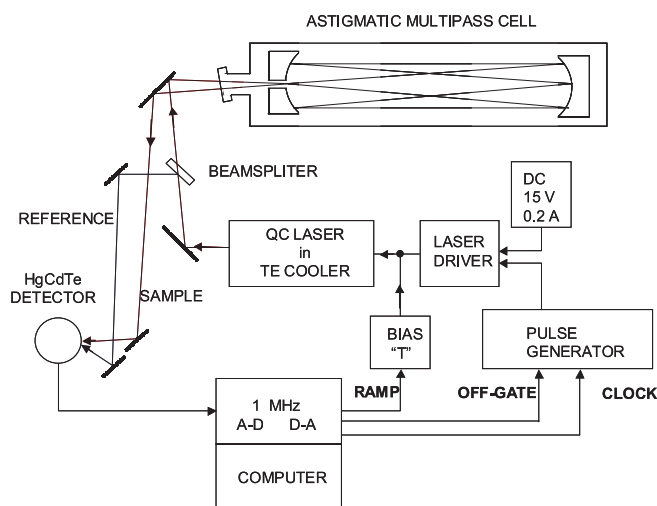


FIGURE 1 Schematic of QC laser spectrometer

2.1 Optical system

The optical system used in this study was adapted from earlier mid-infrared TDL designs [14, 15] with the thermoelectrically cooled unipolar laser housing becoming a drop-in replacement for the liquid-nitrogen laser dewar. The most notable single element of the optical system was a multiple-pass absorption cell with a path length of 210 m and a volume of 5 l, which allows high-sensitivity measurements to be made with sub-second flow response times [16]. The cell is described in more detail below. The laser output, in the form of a broad ($\sim F\# 1$) cone, is collected and transformed into a $F\# 15$ beam by a $15\times$ (Schwarzschild) reflecting objective. The beam is brought to an intermediate focus, which serves as a fixed alignment point for the rest of the optical system, and as a point to observe the laser position using a microscope eyepiece. We also coalign a visible trace beam for alignment purposes, using the first focus as an indexing location. After the first focus, the laser beam is re-imaged into the middle of the absorption cell, with the appropriate magnification to give the very narrow beam ($\sim F\# 50\text{--}100$) that matches the cell recirculation mode. Matching the input beam to the cell mode ensures a minimal beam size within the cell and gives low levels of interference fringes [16].

The optical system also includes a reference path, derived from the portion of the laser beam that reflects from a BaF_2 beam splitter. The reference path is used primarily for pulse normalization, as described below. The reference path is also used to measure the laser tuning rate, by inserting a 25.4-mm germanium etalon, or for absorption-line identification, by inserting a short reference cell containing a low-pressure high-concentration sample of the gas of interest. Both the main (long absorption path) and reference-path beams are directed at a single detector. The TE-cooled detector is a HgCdZnTe photodiode. The liquid-nitrogen-cooled detector is a HgCdTe photodiode. The signals from the two beam paths can be separated temporally. The laser pulses are on the order of 5–10 ns long, the multi-pass absorption cell provides a delay of ~ 700 ns, and both detectors are sufficiently fast (< 70 ns FWHM) to recover between the reference and main signal pulses.

The multi-pass absorption cell is of the astigmatic Herriott type, which offers very long path lengths in a small volume, in a simple and rugged design [16]. The cell used in this study is a variation on the design reported in 1995, with a longer base length (0.88 m) but using mirrors with the same radii of curvature as in the shorter (0.55-m base length) cell. The longer base length requires the selection of a different recirculation pattern, which is quite feasible since there are a great number of available patterns with good optical properties that cover a range of pass numbers from 100 to 300. For a given entrance and exit beam geometry, a unique recirculation pattern can be selected with small adjustments of the cell mirror spacing and the rotation angle of their astigmatic axes.

The uncertainty in the path for a given pattern and set of mirrors with known radii of curvature is less than 1% of the calculated length. Confidence in our calculated length is based in part on comparisons of predicted and observed patterns of the visible trace beam spots on the mirrors, which can be counted for low pass numbers and compared with calculated patterns for higher pass numbers. For high pass number recirculation we observe cell transmission, both intensity and position, consistent with the predicted pass number at the calculated settings of mirror spacing and rotation. Further verification of the path length is provided by the observed absorption due to an added quantity of a gas with known line strength.

The advent of mid-IR lasers with short pulse lengths offers an independent method for validating the calculated path length in the astigmatic cell. We can now directly measure the time delay between light entering and exiting the cell. In Fig. 2 we show an oscilloscope trace of the signal from the single detector with both reference and main pulses. The time delay between the pulses is 708 ± 2 ns, corresponding to a total path length of 212 m. This agrees, within the uncertainty of the timing measurement, to the path length calculated from the identified recirculation pattern (238 passes), the separation between the mirrors of 0.883 m calculated from the mirror radii of curvature for this particular pattern, and the measured

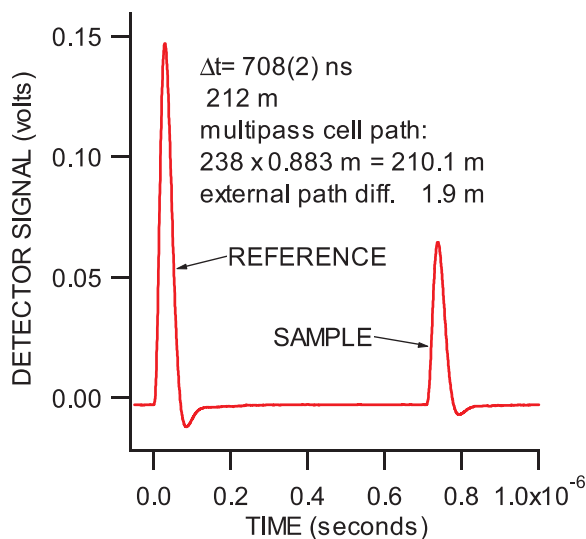


FIGURE 2 Time delay of laser pulse with 210 m multiple pass absorption cell

external path length difference of 1.9 m between the paths of the reference beam and the main beam on the optical table. The flat baseline between the pulses in Fig. 2 confirms that greater than 99.5% of the light emerging from the cell has traveled the specified path length. No light exiting the cell for path lengths other than the specified one is observable.

2.2 Laser control and signal processing system

The data-acquisition system drives the QC lasers, monitors the infrared detector, calculates infrared spectra, analyzes these spectra to derive molecular concentrations, and archives the data. The data-acquisition procedures are implemented using the software package ‘TDLWintel’, originally developed at Aerodyne for cw tunable diode lasers [14, 15] and recently adapted to pulsed QC lasers. The TDLWintel data-acquisition program operates within Microsoft Windows and is designed to frequency scan one or two tunable lasers (pulsed or cw), acquire the resulting absorption spectra, and analyze them by performing an advanced type of sweep integration. In this method, we sweep the laser frequency across the full spectral transition or group of transitions, and then integrate the area under the transitions using non-linear least-squares fitting to the known spectral line shapes and positions. We do not use frequency-modulation (FM) techniques.

For pulsed lasers, each scan is created by repetitively pulsing the laser while simultaneously sweeping its frequency across the desired transition frequency using a software-generated voltage ramp to heat the QC laser. A commercial pulser (Laser Diode Driver, LDD 100, with TTL Pulse Generator TPG 128, both supplied by Alpes Lasers) provided the drive pulses to the laser. The voltage ramp is applied to the QC laser using a bias T. The light pulses are triggered and detected synchronously using a fast (5 MHz) DAC/ADC board which integrates the detector outputs for each pulse. At the end of the scan several laser current pulses are suppressed to determine the detector voltage corresponding to the absence of laser light. Typically, we use a laser pulse rate of 1 MHz, which produces a spectral sweep rate of 10 kHz for a 100-point spectrum. This sweep rate is fast enough to strongly suppress the effects of $1/f$ noise, thus obviating the need for FM detection. Spectra are averaged in a background process while analysis and display are performed in the foreground maintaining a 100% data acquisition duty cycle. The resultant spectrum is fitted in real time to a set of Voigt line shape functions whose line widths and line strengths are derived from the HITRAN spectral database [17] in conjunction with measurements of the pressure and temperature of the sample and the observed laser line width.

By operating the QC laser in pulsed mode, we are able to avoid the use of cryogenic fluids or closed-cycle refrigerators. However, pulsed operation of the lasers does bring two new challenges – broader laser line widths due to the transient heating during the laser pulse and pulse-to-pulse amplitude variation.

The pulse-to-pulse amplitude variation is typically 1 to 2 percent. This can be greatly reduced with signal averaging but is still the largest source of spectral noise if it is left uncorrected. We have therefore implemented a pulse-normalization scheme to reduce the effects of amplitude fluctuation. A refer-

ence laser beam is created using a BaF₂ beam splitter (Fig. 1). This reference beam is sent to the same detector as the signal beam but without traversing the optical multi-pass cell. The signal pulse and the reference pulse arrive at the detector at different times (due to their 212-m path-length difference). Thus a reference spectrum and a signal spectrum are acquired virtually simultaneously. After signal averaging, a normalized spectrum is created by dividing the signal spectrum by the reference spectrum. This procedure can reduce the spectral noise and improve the detectivity by as much as a factor of 10.

The second difficulty associated with pulsing the laser is that it broadens the laser line width. These broader line widths (approximately 4–5 times the Doppler width) reduce spectral resolution and detectivity slightly, but can be tolerated especially at higher sampling pressures. Our efforts to minimize the line width are discussed below. Our present data-processing routines account for the excess line width by approximating the laser line shape as Gaussian. As we will discuss in Sect. 3.1, this approximation is only valid if the laser is operated at a drive voltage just above threshold in order to minimize asymmetrical line broadening due to thermal ‘chirp’. The use of a Gaussian approximation for the laser line shape is computationally convenient since the laser line-shape function may be added in quadrature to the Doppler line-shape function (which is also Gaussian) to produce a combined low-pressure line-shape function. At intermediate pressures, this line-shape function is then convolved with a Lorentzian line-shape function (calculated from the sample pressure and temperature and the HITRAN pressure-broadening coefficients) to produce a Voigt line-shape function, which is an adequate representation of the observed line shape in the optically thin limit.

A typical normalized spectrum during ambient monitoring is shown in Fig. 3. This is a 1-s spectrum of the nitric oxide unresolved doublet at 1897 cm⁻¹ in room air. In this case the laser is pulsed at a rate of 900 kHz, yielding a sweep rate for a 100-point spectrum of 9 kHz. A laser line width of 0.010 cm⁻¹ (HWHM) is determined from a separate, low-pressure spectrum (< 5 Torr), as described in Sect. 3.1.2 below. The laser tuning rate is determined from a germanium etalon. The sampling pressure for ambient monitoring of 48 Torr was chosen to approximately match the pressure-broadened line width to the laser line width. The NO mixing

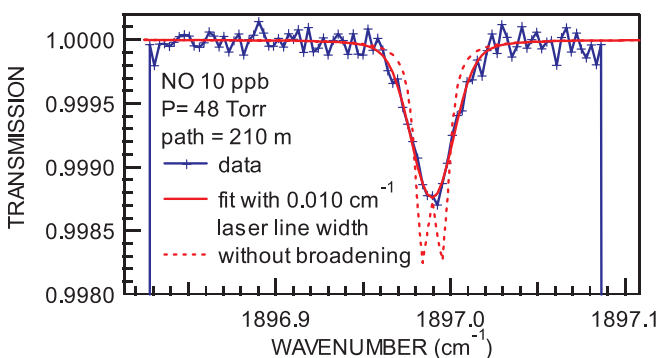


FIGURE 3 Nitric oxide transmission spectrum with 1-s averaging time using TE-cooled laser and detector. The fit is obtained with a laser line width of 0.010 cm⁻¹ HWHM. The simulation without laser broadening for the NO doublet is shown by the dashed line

ratio determined from the spectrum is 10 ppb and the corresponding peak absorption is $\sim 1.3 \times 10^{-3}$.

3 Results

3.1 Laser line width studies

The spectral width and shape of the laser pulse are crucial parameters that determine the applicability and the sensitivity of pulsed quantum cascade lasers for trace-gas detection. Ideally the laser line width should be narrow compared to the absorption line width, resulting in the maximum absorption depth and minimum dependence of the absorbance on the shape of the laser line. This is difficult to achieve with pulsed QC lasers, however, since their output frequency sweeps rapidly during the laser pulse due to the heating by the current pulse. Line widths of 0.005 to 0.05 cm^{-1} (HWHM) have been reported in the literature [8–12] for spectra acquired with pulsed QC lasers. These line widths are significantly larger than typical Doppler widths for small molecules. For instance, the room-temperature Doppler width for NO at 1900 cm^{-1} is 0.002 cm^{-1} (HWHM). We have investigated this problem both empirically and theoretically. On the theoretical side, we have modeled the heat flow in the laser junction to better understand the frequency broadening during a laser pulse. On the empirical side we have varied the current pulses driving the laser in an attempt to reduce the line width.

3.1.1 Thermal modeling of QC lasers. We have modeled the thermal properties of QC lasers in order to better understand the line width under pulsed operation, as well as other thermal tuning issues. The mechanism for generating a finite line width for relatively long pulses is primarily heating during the pulse. The heat changes the refractive index of the laser-active region and causes expansion of the waveguide and overlying grating, causing the laser frequency to sweep, or ‘chirp’. For extremely short pulses ($< 5 \text{ ns}$) there is an additional mechanism for generating a finite line width, which is the broad spectral bandwidth of the pulse itself, referred to as ‘uncertainty broadening’.

Heat-flow calculations in the QC lasers have been performed in one and two dimensions, with both steady-state and time-dependent heat inputs [18, 19]. The steady-state heat calculations yield thermal resistances, the characteristic equilibrium temperature rise per unit heat input. The total thermal resistance of the laser structure is the sum of the thermal resistances for the deposited (active) layers, the InP substrate, and the Cu heat sink. Our result for the total thermal resistance of 3.8 K/W is similar to values reported in the technical literature [20]. Time-dependent heat-flow calculations were used to model the temperature history of the laser over the range of relevant time scales: the duration of the short laser pulse ($\sim 15 \text{ ns}$), the cooling time between pulses ($\sim 2 \mu\text{s}$), and the cycle time of the tuning ramp ($\sim 250 \text{ ms}$).

A numerical model (in one dimension) using the actual QC laser structure [13] was used to study the thermal history of the active region on the time scale of the laser pulses. The model results were in line with expectations from the literature, that very little heat leaves the active region on the time scale of our drive pulses ($\sim 15 \text{ ns}$). On short time scales, the temperature rise of the active region

is well described by the integral of the heat deposited by the drive pulse. The rate of heat deposition in the active region is the input electrical power ($P = I^2 R(I)$) and the rate of temperature rise is also proportional to the power. With a linear tuning rate, the frequency chirp is proportional to the change in active-region temperature during the time that the laser is above threshold. A simple estimate of the thermal chirp line width can be made as follows. With the laser near threshold, we have $V \approx 14$, $I \approx 3.3$, and $\sim 46.2 \text{ W}$ deposited primarily in the active region, with volume $1.9 \times 10^{-7} \text{ cm}^3$ ($1.43 \mu\text{m} \times 44 \mu\text{m} \times 3 \text{ mm}$). The active region is modeled with the thermal properties of $\text{In}_{0.53}\text{Ga}_{0.47}\text{As}$, which has a heat capacity of 0.343 J/g K (at 250 K) and a density of 5.5 g cm^{-3} [21], so the rate of temperature rise is $1.3 \times 10^8 \text{ K/s}$. The laser emission frequency (ν) is set primarily by the DFB grating period (Λ) and the waveguide refractive index (n_g), $\nu = c/(2n_g\Lambda)$. Temperature rise produces a change in the refractive index and hence the emission frequency, with a sensitivity $\nu^{-1} d\nu/dT = -7.6 \times 10^{-5} \text{ K}^{-1}$ (for a laser structure very similar to ours [13]). Thus, for our laser operating near threshold at 1900 cm^{-1} , the chirp rate is $-1.9 \times 10^7 \text{ cm}^{-1}/\text{s}$, or $-0.019 \text{ cm}^{-1}/\text{ns}$. For a pulse that is above threshold for 10 ns , the total chirp would be $\sim 0.19 \text{ cm}^{-1}$. If we assume a parabolic shape for the laser output above threshold as a function of time, we estimate the HWHM line width as $1/2\sqrt{2} \times$ the full chirp. The HWHM line width corresponding to a total chirp of 0.19 cm^{-1} would therefore be $\sim 0.067 \text{ cm}^{-1}$. This simple estimate may be modified by considering electrical power deposition outside the active region and by including explicit time dependence of the electrical pulse, non-linear resistance, and laser output power.

3.1.2 Laser line width measurements. The effect of electrical pulse shape on the laser line width was studied experimentally by collecting a series of absorption spectra while recording the current pulse shape on a digital oscilloscope. Laser instrumental line shapes are determined by recording spectra from a low-pressure (4 Torr) isolated molecular absorption, which is narrow (0.002 cm^{-1} HWHM) compared to the laser line width. A closely spaced multiplet of NO lines at 1894.1 cm^{-1} , which is unresolvable at Doppler resolution, was used in these studies. The linear bias current used to tune the laser results in a quadratic dependence of laser frequency with current since the temperature of the laser junction varies with the change in electrical power. Figure 4 shows a typical NO spectrum and a germanium etalon spectrum recorded simultaneously. The spectral baseline is well approximated with a smooth low-order polynomial function, since most of the variation of laser power with bias current has been removed by normalizing the sample spectrum by the unabsorbed reference spectrum. The etalon spectrum is used to quantify the laser tuning rate function. Knowledge of the tuning rate and the spectral baseline allows us to transform the experimental spectrum to a transmission spectrum as a function of frequency. The laser line shape is obtained by deconvolving the observed transmission spectrum and a synthetic NO transmission spectrum calculated using the HITRAN database parameters at the appropriate pressure and temperature. The deconvolution must be done on the transmission spectrum to conserve the area under

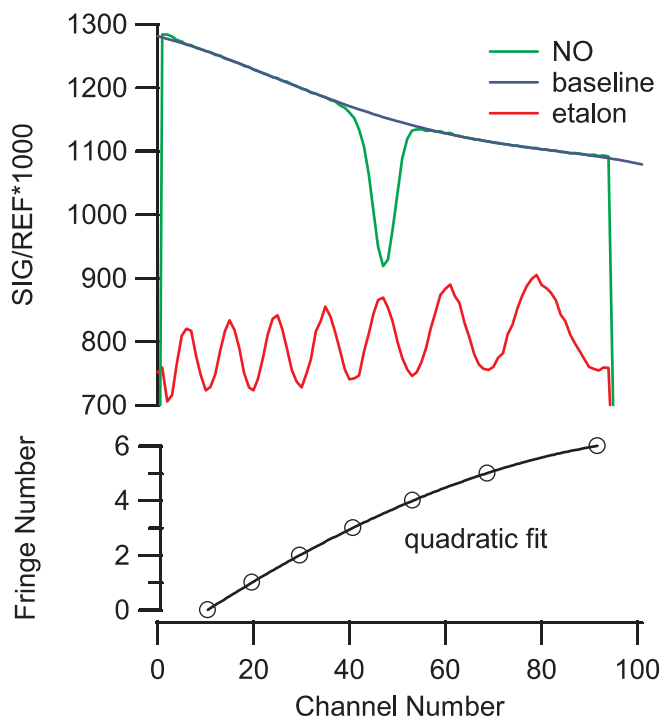


FIGURE 4 Normalized detector signal versus bias current ramp showing absorption by nitric oxide in air at a total pressure of 4 Torr. The output of the current ramp decreased linearly by 0.1 Amp during the sweep. The lower trace shows the fringe pattern obtained with a germanium etalon with a free spectral range of 0.0483 cm^{-1}

the transmission curve. Example spectra for the same NO concentration using two sets of laser drive conditions are shown in Fig. 5. The fits to the data are the result of re-convolving the laser line shapes with the synthetic spectrum.

When the laser line width is much broader than the molecular line width, a good approximation to the laser line width may be obtained simply from the observed spectrum without the deconvolution procedure. Several spectra taken with different pulse energies are displayed in Fig. 6 as absorbances. Each spectrum was signal-averaged for approxi-

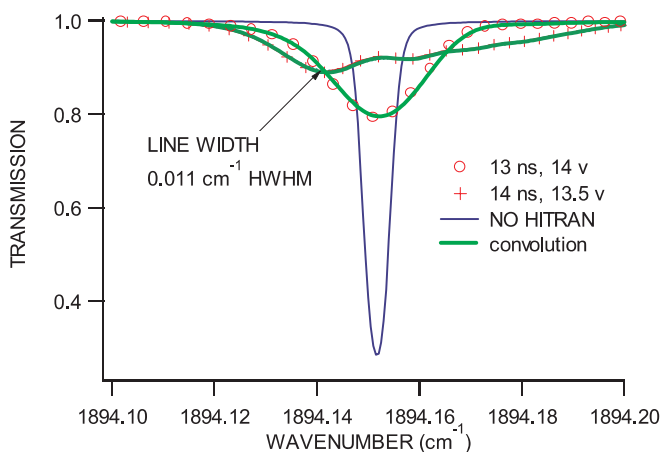


FIGURE 5 Nitric oxide transmission spectra for two laser pulser conditions. The calculated spectrum uses the NO line parameters from HITRAN at the experimental pressure (4 Torr) and temperature (296 K) with the NO column density adjusted to match the area of the experimental transmission spectrum

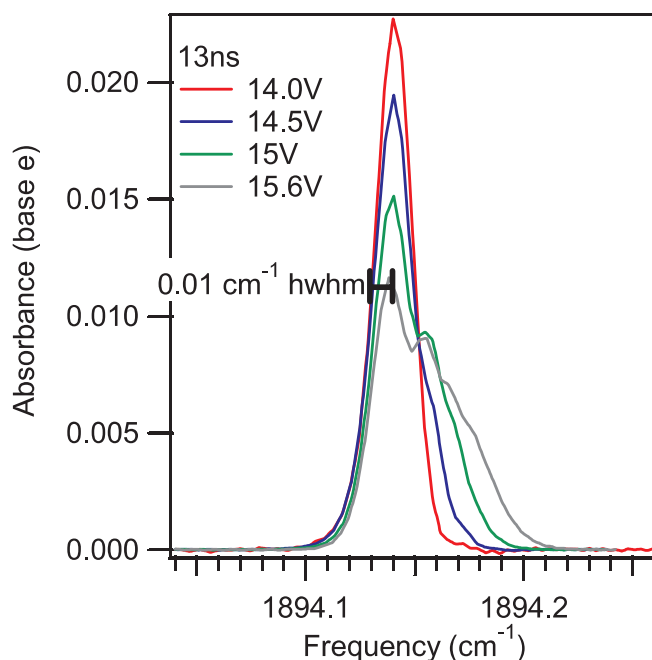


FIGURE 6 Spectra of NO in air ($P = 4\text{ Torr}$) with a pulse width of 13 ns and pulse driver voltages between 14.0 and 15.6 V. The minimum line width is 0.010 cm^{-1} (HWHM)

mately 20 s. These spectra were obtained with a fixed pulse width of 13 ns and supply voltage settings to the pulser unit that varied from 14.0 V to 15.6 V. In all cases the observed line width significantly exceeds the spectral line width by at least a factor of four, so that the instrumental line width is essentially equal to the observed line width. The corresponding electrical pulse shapes were collected using a fast storage oscilloscope with no signal averaging.

The electrical pulse waveforms are shown in Fig. 7. Each of these pulses has a width of $\sim 13\text{ ns}$ (FWHM). The pulses have the same basic shape at all voltages in the range and vary only in amplitude. Each pulse has a rise time on the order of 8 ns, with a slower fall time. The corresponding absorption spectra, however, vary significantly in both width and shape. At higher drive voltages, the spectrum is asymmetric with an overall half-width of 0.020 cm^{-1} (HWHM) but a sharper low-frequency edge with a half-width of only 0.01 cm^{-1} . The narrowest spectrum in Fig. 6, collected at the lowest drive voltage of the series (14.0 V), which is just above threshold, has a half-width of 0.010 cm^{-1} (HWHM). As the drive voltage is increased, the width of the line increases rapidly.

The rapid increase of line width with drive voltage is associated with a sharp increase in the lasing duration. The laser is above threshold for a longer time and is therefore swept further in frequency. We estimate that the lowest-voltage pulse (with line width 0.01 cm^{-1} HWHM) is only above threshold for approximately 4–5 ns, whereas the highest-voltage (15.6 V) pulse (with line width 0.022 cm^{-1} HWHM) is above threshold for 7–8 ns. The spectra acquired with higher drive voltages are also asymmetric with broad tailing to the high-frequency side. This implies that the laser frequency distribution is also asymmetric with tailing to the low-frequency side. The observed current pulses do not readily explain this asymmetry – that is, they do not show marked asymmetry. We

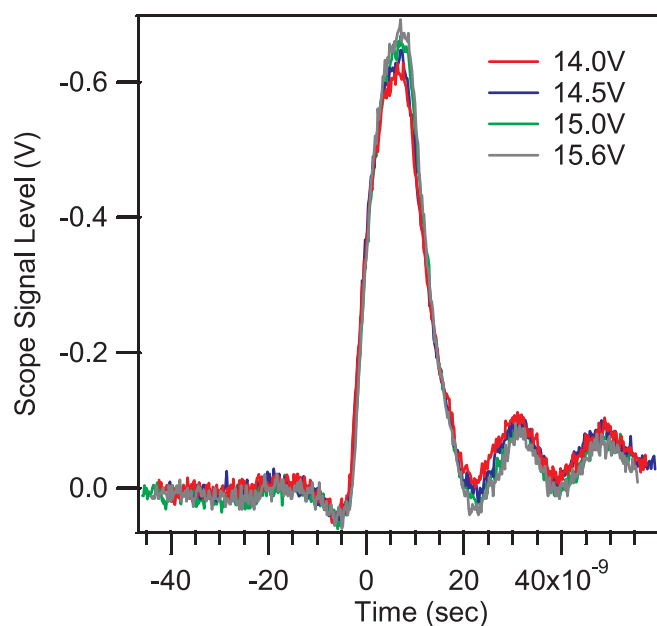


FIGURE 7 Electrical pulse shapes applied to the laser corresponding to spectra in Fig. 6. The actual voltages to the laser are 10 times greater than the voltage observed on the oscilloscope

are continuing to investigate this phenomenon. An important unanswered question is whether this frequency distribution is a property of an individual pulse or whether it is due to pulse-to-pulse frequency jitter – which could result in an apparent asymmetric shape after averaging of several thousand spectra. The measured line widths are smaller by a factor of 1/2 than the simple chirp estimate given in Sect. 3.1.1. If the laser were above threshold for 7.5 ns (15.6-V pulse), the estimated chirp is 0.05 cm^{-1} HWHM, while the measured value is 0.022. The discrepancy could be due in part to the assumption that all of the electrical power is deposited in the active layer, as well as uncertainties in the thermal constants in the model.

Our observed line widths are among the sharpest reported in the literature to date, especially when expressed as a fraction of the laser frequency. This is a sensible way to report the line width since a given amount of thermal expansion will chirp the laser by an amount proportional to its lasing frequency. In these terms, the 0.010-cm^{-1} line width reported above corresponds to a fractional line width of 5×10^{-6} (HWHM). Literature values for the fractional line width range from 4×10^{-6} to 25×10^{-6} [8–12] with the best previous results reported by Kosterev et al. [9] using ~ 5 -ns pulses. The line widths observed here are narrow due to the fact that we are operating close to threshold and therefore with minimum power output from the laser and a lasing duration which is brief compared to the pulse duration. There is a strong trade-off between high output powers and narrow line widths for optimizing sensitivity for a given optical system and detection approach. This is shown in Figs. 5 and 6 where the peak absorbance decreases proportionally to laser line width while the laser power (not shown) increases substantially for the higher pulse voltages. The pulse energy collected by the signal detector using the 14-V drive voltage was only $\sim 0.3 \text{ pJ}$, which corresponded to an average power of $\sim 300 \text{ nW}$. We estimate, from the optical collection effi-

ciency (~ 0.1) and the multi-pass cell transmission efficiency (~ 0.1), that the average output power of the laser was no more than $30 \mu\text{W}$ for the narrowest line widths. By increasing the drive voltage, we can easily collect 10 times more power at the expense of the instrumental line width.

We are continuing to investigate methods for generating short ($< 5 \text{ ns}$) pulses at high repetition rate and with excellent stability in order to further improve our detection sensitivity and spectral resolution. However, we do not expect dramatic further improvements in line width with these lasers, since we are clearly close to the transform limit for spectral resolution with 4–5 ns pulses. By approximating the part of the pulse above threshold as a Gaussian with 2.5-ns width (FWHM), we estimate that the uncertainty broadening associated with these pulses is 0.003 cm^{-1} . If we assume that the laser chirp is linear with time and that the two broadening mechanisms can be added in quadrature, then a minimum line width of 0.007 cm^{-1} might be achievable with a 1.4-ns Gaussian drive pulse (FWHM) for lasers operating near 1900 cm^{-1} . This would correspond to a fractional spectral resolution of 4×10^{-6} (HWHM) for operation just above threshold. In fact, we have observed narrower line widths (0.007 cm^{-1} HWHM) with a prototype faster pulse driver from Alpes Laser but we did not achieve an improved detection limit with this driver. This may be due to increased amplitude variability in the pulse train. Thus, the NO ambient monitoring results reported in Sect. 3.2 used the original Alpes Laser pulse driver and its associated spectral resolution of 0.010 cm^{-1} .

An ideal pulse driver circuit would operate with an electrical pulse width which matches thermal broadening and uncertainty broadening. It should have a fast rise and fall time to maximize the operating voltage while minimizing the lasing duration. This would allow increased laser output power while maintaining better overlap between the instrumental width and the molecular line width to maximize sensitivity. Alternative pulse driver circuits are presently being investigated which could provide substantial increases in laser power output while maintaining narrow line widths.

3.2 Ambient monitoring of NO

We have employed the QC system for ambient monitoring of nitric oxide. The unresolved doublets at either 1900.08 cm^{-1} or 1896.98 cm^{-1} were used with similar results. A sampling pressure of 48 Torr was chosen to approximately match the pressure-broadened line width to the laser line width. Each spectrum is similar to the one shown in Fig. 3. A time series of the results of successive fits of 1-s spectra is shown in Fig. 8. The figure shows only two small portions of an extended one-month period of continuous sampling of ambient air from the Aerodyne rooftop. The time series on the left-hand side of Fig. 8 highlights a region with low NO mixing ratios, while the data on the right-hand side has high NO events. The time series in Fig. 8 shows the influence of vehicular traffic from a nearby highway and a local delivery truck on ambient NO mixing ratios. The QCL and TDL instruments concurrently measure NO in the outside air using separate but collocated sampling tubes. Zero air from a cylinder of compressed nitrogen was introduced into the sampling system at 15-min intervals. The measurement precision of

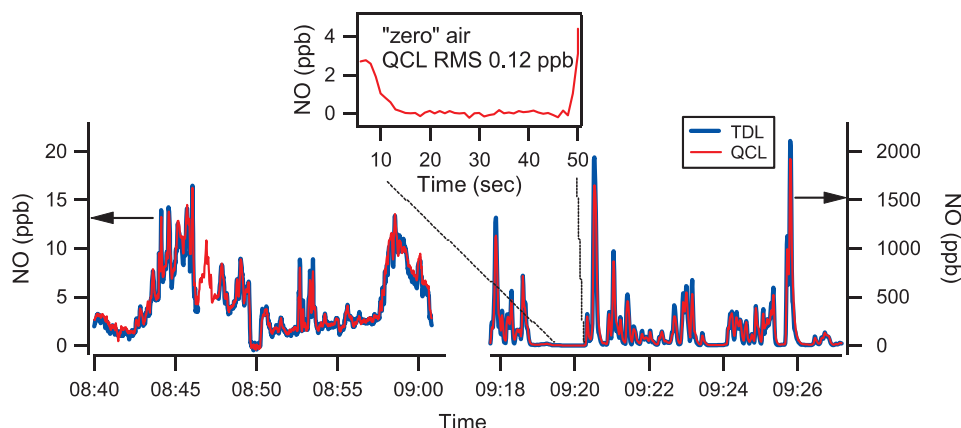


FIGURE 8 Nitric oxide from local vehicle traffic sampled from Aerodyne rooftop comparing results for QCL and TDL spectrometers at low concentrations (*left*) and high concentrations (*right*). The *inset* shows the precision for the QCL system during 'zero' gas addition to the inlet

the QCL system may be obtained during these zero additions and is $0.12 \text{ ppb Hz}^{-1/2}$ (1σ) when using the liquid-nitrogen-cooled HgCdTe detector. This corresponds to an absorbance precision of $1 \times 10^{-5} \text{ Hz}^{-1/2}$ based on the correspondence between mixing ratio and peak absorbance determined from the simulation in Fig. 3 with a laser line width of 0.01 cm^{-1} . The corresponding absorbance per path length with the 210-m multiple-pass cell is $5 \times 10^{-10} \text{ cm}^{-1} \text{ Hz}^{-1/2}$.

During a portion of the measurement period, the data could be compared directly with a dual tunable diode laser system [15] operating with a lead-salt tunable diode in cw mode. The optical layouts for the two systems are similar. The TDL system used a multiple-pass cell set for 150-m path length, and used the NO transitions at 1896.98 cm^{-1} with a lower sampling pressure of 25 Torr. The TDL system used continuous peak locking to a reference cell, periodic background subtraction with 'zero' air addition (e.g. the gap in the TDL data at $\sim 08:47$ in Fig. 8), and a heated and thermostated optical table to minimize baseline drifts due to changes in optical interference fringes. The QCL system operated on a laboratory cart without thermal stabilization of the optical system. The optical fringes in the pulsed QCL system appeared to be substantially reduced compared to the TDL system. Instrumental zero drift was $\pm 2 \text{ ppb}$ with a typical drift rate of $< 1 \text{ ppb/h}$. The two instruments compare very well over a wide range of ambient mixing ratios from 1 to 2000 ppb. The mixing ratios reported by the TDL and the QCL over the time period plotted in Fig. 8 are compared in Fig. 9 by plotting the NO concentration determined by the QCL system against that determined by the TDL system. There is good correlation over more than three orders of magnitude in mixing ratios with no apparent deviation from linearity even at relatively high absorbance. A linear regression slope of 0.931 ± 0.002 is obtained, which is in reasonable agreement considering that the calibration of both systems is based totally upon the spectroscopic constants and the fitting procedures as described in Sect. 2. Since the spectroscopic constants both come from the HITRAN database [17], the greatest relative errors in this comparison are due to the uncertainties in the determination of the QC laser line width and approximations used in the fitting program for the QC line shape and tuning rate function.

The majority of the ambient measurements were conducted using a thermoelectrically cooled HgCdZnTe detec-

tor, since it permitted totally cryogen-free operation, which is especially convenient for extended monitoring. The detector noise was a factor of two to four greater for this detector compared to the liquid-nitrogen-cooled detector. The bandwidth for the TE-cooled detector was also sufficiently fast to perform pulse normalization with a single detector, as is shown in the oscilloscope trace in Fig. 2. (Both Figs. 2 and 3 were recorded using the TE-cooled detector.) A time-series trace is shown in Fig. 10 for an 18-h period. A precision of $0.3 \text{ ppb Hz}^{-1/2}$ (1σ) is obtained from the variations observed during short periods of relative stability in the ambient NO or while sampling laboratory room air. The CO_2 trace shown in Fig. 10 was recorded with a non-dispersive infrared analyzer and shows a strong correlation between NO and CO_2 , which indicates combustion as the local source of NO. The totally cryogen-free mid-IR system will greatly simplify the opera-

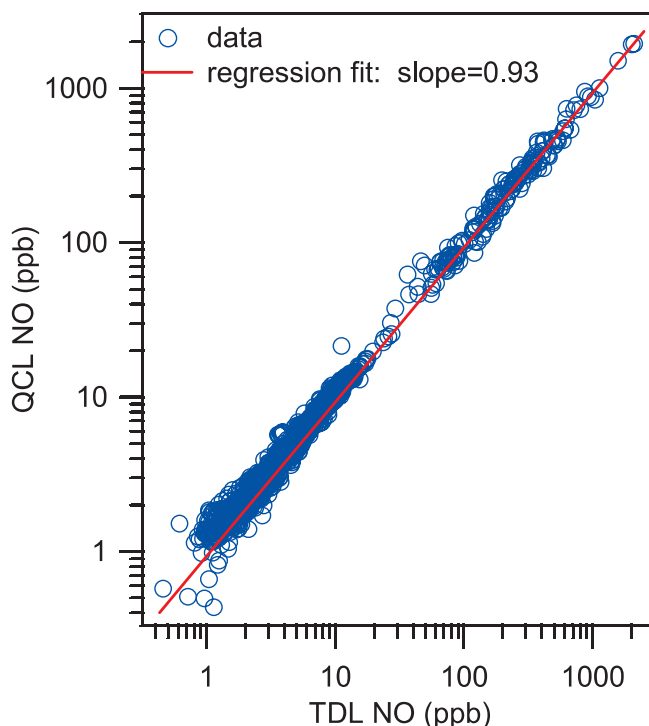


FIGURE 9 Comparison of NO concentrations from QCL and TDL instruments for the data shown in Fig. 8

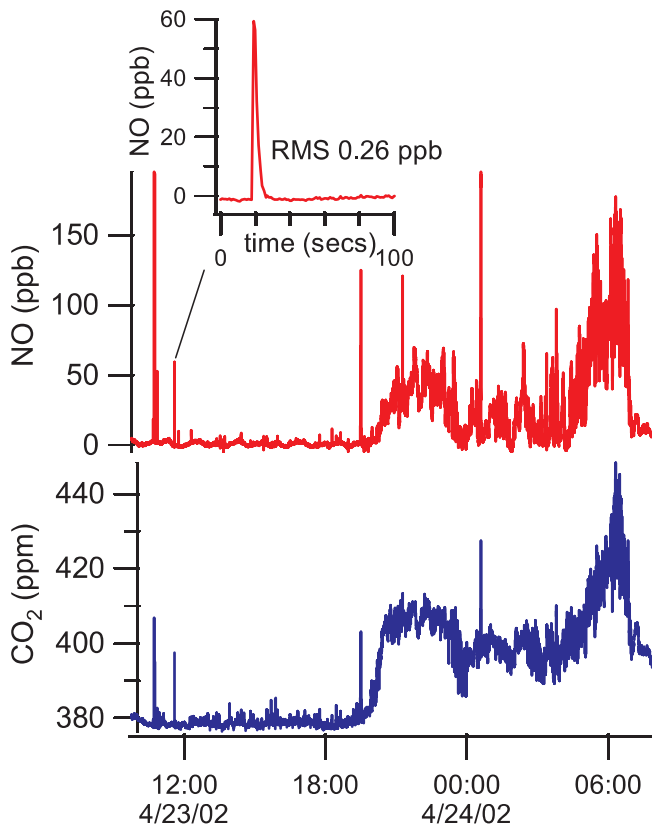


FIGURE 10 NO mixing ratios obtained with TE-cooled QCL spectrometer and detector. The lower trace shows CO₂ data obtained with a non-dispersive infrared monitor

tion logistics of using mid-IR absorption for urban emission monitoring compared to using lead-salt TDLs [22].

4 Abstract and conclusions

Detection of nitric oxide in the atmosphere with a mixing ratio less than 1 nmole/mole (ppb) has been demonstrated using mid-infrared absorption with a unipolar (quantum cascade) laser operating in the pulsed mode with thermoelectric cooling of laser and detector. High sensitivity is obtained in the pulsed mode by (i) coupling the laser to a long path length (210 m) multiple-pass absorption cell, (ii) operating the laser near threshold to minimize laser line width, and (iii) reducing the effects of pulse-to-pulse amplitude variations by normalizing each spectrum to a reference spectrum recorded simultaneously on the same detector element. A precision of $0.3 \text{ ppb Hz}^{-1/2}$ (1σ) is obtained using a TE-cooled detector, limited mainly by detector noise. With a more sensitive liquid-nitrogen-cooled detector, a precision of $0.12 \text{ ppb Hz}^{-1/2}$ is obtained, limited by a combination of detector noise and residual pulse-to-pulse amplitude variations. This corresponds to an absorbance precision of $1 \times 10^{-5} \text{ Hz}^{-1/2}$ or an absorbance per path length of $5 \times 10^{-10} \text{ cm}^{-1} \text{ Hz}^{-1/2}$.

The ability to operate a mid-infrared laser spectrometer continuously without cryogenic cooling opens up numer-

ous possibilities for long-term environmental measurements. Other trace gases detectable with this technique include nitrogen dioxide, ozone, carbon monoxide, formaldehyde, methane, nitrous oxide, sulphur dioxide, ammonia, and nitric acid as unipolar or quantum cascade lasers become more widely available at the requisite wavelengths.

ACKNOWLEDGEMENTS We gratefully acknowledge the technical advice and assistance of Antoine Müller and Daniel Hofstetter from Alpes Lasers and the University of Neuchatel. Funding for this work was provided in part by the Small Business Innovation Research Programs of the U.S. Department of Energy (Contract No. DE-FG02-01ER83139), the U.S. Environmental Protection Agency (Contract No. PR-NC-00-10447), and the National Aeronautics and Space Administration (Contract No. NAS3-01010).

REFERENCES

- 1 J. Faist, F. Capasso, D.L. Sivco, C. Sirtori, A.L. Hutchinson, A.Y. Cho: *Science* **264**, 508 (1994)
- 2 F. Capasso, C. Gmachl, A. Tredicucci, A.L. Hutchinson, A.Y. Cho: *Opt. Photon. News* **10**, 31 (1999)
- 3 F. Capasso, C. Gmachl, A. Tredicucci, A.L. Hutchinson, A.Y. Cho: *Phys. World* **12**, 27 (1999)
- 4 C. Gmachl, F. Capasso, J. Faist, A.L. Hutchinson, A. Tredicucci, D.L. Sivco, J.N. Baillargeon, S.N.G. Chu, A.Y. Cho: *Appl. Phys. Lett.* **72**, 1430 (1998)
- 5 S.W. Sharpe, J.F. Kelly, J.S. Hartman, C. Gmachl, F. Capasso, D.L. Sivco, J.N. Baillargeon, A.Y. Cho: *Opt. Lett.* **23**, 1396 (1998)
- 6 C.R. Webster, G.J. Flesch, D.C. Scott, J.E. Swanson, R.D. May, W.S. Woodward, C. Gmachl, F. Capasso, D.L. Sivco, J.N. Baillargeon, A.L. Hutchinson, A.Y. Cho: *Appl. Opt.* **40**, 321 (2001)
- 7 J.B. Paul, L. Lapson, J.G. Anderson: *Appl. Opt.* **40**, 4904 (2001)
- 8 K. Namjou, S. Cai, E.A. Whittaker, J. Faist, C. Gmachl, F. Capasso, D.L. Sivco, A.Y. Cho: *Opt. Lett.* **23**, 219 (1998)
- 9 A.A. Kosterev, F.K. Tittel, C. Gmachl, F. Capasso, D.L. Sivco, J.N. Baillargeon, A.L. Hutchinson, A.Y. Cho: *Appl. Opt.* **39**, 6866 (2000)
- 10 D.M. Sonnenfroh, W.T. Rawlins, M.G. Allen, C. Gmachl, F. Capasso, A.L. Hutchinson, D.L. Sivco, J.N. Baillargeon, A.Y. Cho: *Appl. Opt.* **40**, 812 (2001)
- 11 D. Hofstetter, M. Beck, J. Faist, M. Nagele, M.W. Sigrist: *Opt. Lett.* **26**, 887 (2001)
- 12 A.A. Kosterev, F.K. Tittel, R. Kohler, C. Gmachl, F. Capasso, D.L. Sivco, A.Y. Cho, S. Wehe, M.G. Allen: *Appl. Opt.* **41**, 1169 (2002)
- 13 D. Hofstetter, M. Beck, T. Allen, J. Faist: *Appl. Phys. Lett.* **78**, 396 (2001)
- 14 M.S. Zahniser, D.D. Nelson, J.B. McManus, P.L. Kebedian: *Philos. Trans. R. Soc. Lond. A* **351**, 357 (1995)
- 15 C.V. Horii, M.S. Zahniser, D.D. Nelson, J.B. McManus, S.C. Wofsy: *SPIE Proc.* **3758**, 152 (1999)
- 16 J.B. McManus, P.L. Kebedian, M.S. Zahniser: *Appl. Opt.* **34**, 3336 (1995)
- 17 L.S. Rothman, C.P. Rinsland, A. Goldman, S.T. Massie, D.P. Edwards, J.-M. Flaud, A. Perrin, C. Camy-Peyret, V. Dana, J.-Y. Mandin, J. Schroeder, A. McCann, R.R. Gamache, R.B. Wattson, K. Yoshino, K.V. Chance, K.W. Jucks, L.R. Brown, V. Nemtchinov, P. Varanasi: *J. Quantum Spectrosc. Radiat. Transfer* **60**, 665 (1998)
- 18 H.S. Carslaw, J.C. Jaeger: *Conduction of Heat in Solids* (Oxford University Press, Oxford 1948)
- 19 W.H. Press, S.A. Teukolsky, W.A. Vetterling, B.P. Flannery: *Numerical Recipes* (Cambridge University Press, Cambridge 1992)
- 20 C. Gmachl, A.M. Sergent, A. Tredicucci, F. Capasso, A.L. Hutchinson, D.L. Sivco, J.N. Baillargeon, S.N.G. Chu, A.Y. Cho: *IEEE Photon. Technol. Lett.* **11**, 1369 (1999)
- 21 V. Palankovski: PhD Dissertation, Technical University of Vienna 2000
- 22 D.D. Nelson, M.S. Zahniser, J.B. McManus, C.E. Kolb, J.L. Jimenez: *Appl. Phys. B* **67**, 433 (1998)